Deep-Sea Research, 1976, Vol. 23, pp. 413 to 427. Pergamon Press. Printed in Great Britain.

The interaction of zonal currents with topography with applications to the Southern Ocean*

M. S. McCartney†

(*Received* 10 *March* 1975; *in revised form* 5 *August* 1975; *accepted* 5 *September* 1975)

Abstract—An analytical model for the interaction of a broad, eastward baroclinic current with shallow topographic features in an unbounded β-plane ocean is developed and solved for three types of topography: a meridionally oriented ridge as is found in the central South Pacific and South Atlantic sectors of the Southern Ocean, a zonally oriented ridge as is found south of Australia and Africa, and an isolated plateau or seamount. The meridional ridge causes a stationary wave pattern similar to that believed to occur in the southeast Pacific Ocean. The zonal ridge causes a current intensification on the equatorward side of the ridge crest, with intermittent slowed or reversed flow and a string of stationary warm core eddies on the poleward side. Comparison is made to Callahan's (1971, *Journal of Geophysics Research*, **76**, 5859–5870) observations of the flow along the ridge south of Australia. The isolated seamount forces a Taylor column (warm core anticyclonic eddy) above it, and has a stationary meandering wake downstream, sometimes with embedded eddies.

1. INTRODUCTION

Several recent papers discuss physical oceanographic observations in the Southern Ocean and establish some interesting correlations between the spatial distributions of quantities like dynamic height and the rugged bottom topography of the region. In the present work an attempt to understand the role of current–bottom topography interaction in Southern Ocean dynamics will be presented. The model describes the finite amplitude steady disturbances to a horizontally uniform, vertically sheared, eastward stratified current caused by its interacting with several types of simple shallow topographic features.

2. FORMULATION

The basic flow field will be characterized by a root-mean-square speed U_r:

$$U_r = \left[\frac{1}{H}\int_0^H U^2(z')\lambda z'\right]^{\frac{1}{2}}, \qquad (2.1)$$

where $U(z')$ represents a meridionally averaged zonal velocity at a height above sea floor of z' and H is the mean depth. In the absence of currents the water column is characterized by a total density variation $\Delta\rho$ and a mean density ρ_r. The topography will be characterized by a single horizontal scale L and a height h_0'. The β-plane will be used throughout: $f(y') = f_0 + \beta y'$, with y' being the poleward directed coordinate.

The nondimensional parameters characterizing the problem are:

$$\varepsilon = \frac{U_r}{f_0 L} \quad h_0 = \frac{h_0'}{H} \quad \delta = \frac{H}{L}$$

$$S = (\delta N/f_0)^2 = \frac{gH}{f_0^2 L^2}\frac{\Delta\rho}{\rho_r} \quad b = \frac{\beta L^2}{U_r} \qquad (2.2)$$

with N = Brunt–Väisälä frequency.

*Woods Hole Oceanographic Institution Contribution Number 3539.

†Woods Hole Oceanographic Institution, Woods Hole, Massachusetts 02543, U.S.A.

A value of $U_r = 5$ cm s^{-1} seems to be consistent with CALLAHAN's (1971) transport measurements south of Australia. For $\beta = 1{\cdot}5 \times 10^{-13}$ s^{-1} cm^{-1}, $\Delta\rho/\rho_r < 10^{-3}, f_0 = 10^{-5}$ s^{-1}, $H = 5$ km, and restricting $L > 100$ km gives $\varepsilon < 5 \times 10^{-3}$, $S < 10^{-1}$, $\delta < 10^{-2}$, and $b > 3$. Analytically it proves convenient to assume $S \ll 1$; for $L = 100$ km this is marginal. However, the observations that will be compared to the model results generally have L larger than this. For example, in CALLAHAN's (1971) observation of flow along a submarine ridge south of Australia, the ridge scale, defined by $L = H/H_{y'}$, is greater than 100 km. The following analysis formulates a model under the assumptions:

$$S \ll 1,\ \varepsilon \ll 1,\ \delta \ll 1 \qquad b = 0(1) \quad h_0 = 0(\varepsilon). \tag{2.3}$$

The pressure and density fields are split into dynamic and hydrostatic components:

$$p' = p_0' + \rho_r U_r f_0 L p_s(z) + p(x, y, z)$$
$$\rho' = \rho_0' + \left[\rho_s(z) + \frac{\varepsilon}{S}\rho(x, y, z)\right]\Delta\rho, \tag{2.4}$$

where p_0' and ρ_0' are the pressure and density at $z = 0$ in the absence of any motion, and p_s and ρ_s are the nondimensional hydrostatic fields in the absence of any motion and are related by the hydrostatic relation

$$\frac{dp_s}{dz} = -\frac{S}{\varepsilon}\left[\frac{\rho_0'}{\Delta\rho} + \rho_s(z)\right]. \tag{2.5}$$

S and ε were defined in equations (2.2); x and y are the eastward and poleward coordinates, scaled by L; z is the vertical coordinate zero at the bottom, positive upwards, scaled by the mean depth H. The separation giving ρ_0, $\Delta\rho$, and $\rho_s(z)$ is such that $\rho_s(0) = 0$ and $\rho_s(1) = 1$, hence $\Delta\rho$ gives the total static density range. p and ρ are the nondimensional dynamic pressure and density. Scaling horizontal velocities by U_r, vertical velocity by $U_r\delta$ with $\delta \equiv H/L$, and using the β-plane $f(y) = f_0(1 + \varepsilon by)$, the nondimensional equations of motion for an inviscid Boussinesq fluid are:

$$\varepsilon\,\mathbf{q}\cdot\nabla u - (1 + \varepsilon by)v = -p_x,$$
$$\varepsilon\,\mathbf{q}\cdot\nabla v + (1 + \varepsilon by)u = -p_y,$$
$$\varepsilon\delta^2\mathbf{q}\cdot\nabla w = -p_z - \rho, \tag{2.6}$$
$$\varepsilon\,\mathbf{q}\cdot\nabla\rho + Sw\frac{d\rho_s}{dz} = 0, \text{ and}$$
$$\nabla\cdot\mathbf{q} = 0,$$

$\mathbf{q}$ being the nondimensional velocity vector and ∇ the three-dimensional divergence operator.

For small Rossby number, the dependent variables are expanded in powers of ε, e.g. $u = u^{(0)} + \varepsilon^1 u^{(1)} + \ldots$ The order ε^0 balances are:

$$-v^{(0)} = -p_x{}^{(0)},$$
$$u^{(0)} = -p_y{}^{(0)},$$
$$\rho^{(0)} = -p_z{}^{(0)}, \tag{2.7}$$
$$\nabla\cdot\mathbf{q}^{(0)} = 0, \text{ and}$$
$$\mathbf{q}^{(0)}\cdot\nabla\rho^{(0)} = -\frac{S}{\varepsilon}\frac{d\rho_s}{dz}[w^{(0)} + \varepsilon w^{(1)}].$$

Equations (2.7) can be manipulated to give:

$$w^{(0)} = 0,\ u_z{}^{(0)} = \rho_y{}^{(0)},\ v_z{}^{(0)} = -\rho_x{}^{(0)},$$
$$\rho^{(0)} = -p_z{}^{(0)}, \tag{2.8}$$

and hence, for $S \ll 1$

$$\mathbf{q}^{(0)}\cdot\nabla\rho^{(0)} = -\mathbf{q}^{(0)}\cdot\nabla p_z{}^{(0)} = 0. \tag{2.9}$$

Equation (2.9) can be written in Jacobian form

$p_y{}^{(0)}\,p_{xz}{}^{(0)} - p_x^{(0)}\,p_{yz}{}^{(0)} = 0$, and integrated once to give:

$$p_z^{(0)} = F[p^{(0)}]. \tag{2.10}$$

Assuming all streamlines originate upstream and the flow upstream to be:

$$p^{(0)} \to -U_0(z)y, \tag{2.11}$$

i.e. a horizontally uniform, vertically sheared, eastward directed [for $U_0(z) > 0$] current, then $F[p^{(0)}]$ in equation (2.10) is

$$F[p^{(0)}] = \left[\frac{U_0'(z)}{U_0(z)}\right] p^{(0)}. \tag{2.12}$$

Substituting $F[p^{(0)}]$ into equation (2.10) and integrating in z gives:

$$p^{(0)} = U_0(z)\psi(x, y). \tag{2.13}$$

The separable z dependence means that the horizontal streamline and isopycnal patterns are independent of z. For example, using the thermal wind relation in equation (2.8) gives

$$\begin{aligned} \mathbf{q}^{(0)} &= U_0(z)\,[-\psi_y \hat{\imath} + \psi_x \hat{\jmath}] \\ &\equiv U_0(z)\mathbf{u}(x, y), \end{aligned} \tag{2.14}$$

indicating that the velocity vector changes in magnitude but not in direction with z.

The order ε^1 balances yield a vorticity equation:

$$\mathbf{q}^{(0)} \cdot \nabla[\nabla_h^2 p^{(0)} + by] = w_z^{(1)}, \tag{2.15}$$

where ∇_h^2 is the horizontal Laplacian operator. Equation (2.15) can be vertically integrated, because the z dependence of $p^{(0)}$ and $\mathbf{q}^{(0)}$ are known by equation (2.13) and equation (2.14). At $z = 1$, $w^{(1)}$ is zero, while at $z = h \simeq 0$ [$h = 0(\varepsilon)$], $w^{(1)} = \mathbf{q}^{(0)} \cdot \nabla \frac{h}{\varepsilon}$.

$$\mathbf{u} \cdot \nabla\left[\nabla_h^2\psi + b\,\bar{U}_0 y + U_0(0)\frac{h}{\varepsilon}\right] = 0, \tag{2.16}$$

where

$$\bar{U}_0 = \int_0^1 U_0(z)\mathrm{d}z. \tag{2.17}$$

Note that $U_0(z)$ is scaled by U_r so $\int_0^1 U_0^2 \mathrm{d}z = 1$.

Equation (2.16) can be treated in the same manner as equation (2.9): written in Jacobian form, integrated, and the arbitrary function of ψ determined by knowledge of the upstream relation $\psi = -y$. Writing $\psi = -y + \varphi(x, y)$, this yields:

$$\nabla_h^2\varphi + b\,\bar{U}_0\varphi = -U_0(0)\frac{h}{\varepsilon}. \tag{2.18}$$

Several comments can be made about equation (2.18). First, it is the same equation one obtains for the stream function for the corresponding homogeneous fluid problem, where $\bar{U}_0 = U_0(0) = 1$. The only effect of stratification in the $S = 0(\varepsilon)$ formulation is to allow vertical shear via $U_0(z)$. Secondly, the operator on the left-hand side of equation (2.15) is wavelike for $\bar{U}_0 > 0$, evanescent for $\bar{U}_0 < 0$, i.e. depending on the sign of the depth averaged approaching velocity. Thirdly, if there is no bottom velocity [$U_0(0) = 0$] then the current does not feel the bottom ($\varphi \equiv 0$).

In the following sections, solutions to equation (2.18) will be presented for three types of topography: a meridional ridge, a zonal ridge, and an isolated seamount. In the latter two cases, for sufficiently high topography, the solutions to equation (2.18) will correspond to closed ψ contours, and the steps leading from equation (2.10) to equation (2.12) and from equation (2.16) to equation (2.18) break down because all streamlines do not now originate upstream where $\psi = -y$. In the framework of a temporal initial value problem such closed contours contain fluid, originally connected to streamlines originating upstream, which was trapped within a growing meander, closed upon itself, and

pinched off. The solutions to equation (2.18) then represent the ultimate steady state that such an inviscid process would tend to. Ingersoll (1969) argued that with small bottom friction the ultimate state within such closed streamlines must be stagnation and was able to modify his f-plane Taylor column solution to take this into account. In the solutions to be presented, this modification is not possible, so they must be considered to be solutions corresponding to times short compared to the viscous time scale.

3. Meridional Ridges

There have been several previous theoretical studies concerning the interaction of a horizontally uniform zonal barotropic current with bottom topography that varies only in the downstream direction. Neumann (1960) formulated the problem in terms of a linear bottom frictional beta-plane model. This model contains as special cases the Ekman (1923) model ($\beta \equiv 0$) and the Sverdrup (1941) model (zero bottom friction). For a Gaussian ridge the Ekman model indicates a streamline deflection that is anticyclonic on the upstream half and cyclonic on the downstream half with a net streamline deflection. The Sverdrup model for the same geometry gives first, anticyclonic deflection upstream of the ridge crest, cyclonic over the ridge crest, then anticyclonic downstream of the ridge crest; there is no net streamline deflection. Neumann's solutions show a mixture of these two effects.

The papers by Porter and Rattray (1964), McIntyre (1968), and Clark and Fofonoff (1969) recognized that relative vorticity effects are generally as important as β-effects in typical ocean situations. Taking this into account gives a nonlinear potential vorticity conservation equation. Finite amplitude disturbance solutions are presented for various examples of downstream varying topography, their main feature (for eastward directed flow) being the existence of stationary Rossby waves downstream of the topography (or over the topography in the case of a step profile). The present model, with $h = h(x)$, can be regarded as baroclinic extension of this group of barotropic models.

For topography of the form $h = h(x)$ in an ocean unbounded in y, $\varphi = \varphi(x)$, hence the governing equation becomes

$$\varphi'' + b\bar{U}_0\varphi = -U_0(0)h/\varepsilon. \tag{3.1}$$

Equation (3.1) is just a forced spring equation with x playing the role of time, φ the role of spring deflection, and h the forcing. There is no damping (which for simple bottom friction would be proportional to φ'), so even if $h(x)$ vanishes downstream of some location, any oscillations set up by the forcing persist there. It can be shown that any stationary waves set up by the interaction with the topography occur downstream (to the east) from the topography; see Lighthill (1966).

As an example, the solution corresponding to

$$h = h_0 e^{-|x|}, \tag{3.2}$$

and satisfying the no upstream wave condition is

$$\varphi = -U_0(0)\,\frac{h_0}{\varepsilon}\,\frac{1}{1 + b\bar{U}_0}$$

$$\begin{cases} e^{x} & x < 0 \\ e^{-x} + 2(b\bar{U}_0)^{-\frac{1}{2}}\sin[(b\bar{U}_0)^{\frac{1}{2}}x] & x > 0 \end{cases} \tag{3.3}$$

Equation (3.3) gives φ and φ' that are continuous, but φ'' is discontinuous at $x = 0$; this is because of the cusp nature of h: a smoothly varying h has a correspondingly smoothly varying φ. Streamlines corresponding to equation (3.3) with $b\bar{U}_0 = 1$ are shown (Fig. 1) for $U_0(0)\,h_0/\varepsilon = 2$. To put the streamline pattern in perspective, recall the familiar concept of a noninertial barotropic current following lines of constant f/H. In the present formulation this is equivalent to following the lines of $b\bar{U}_0 y + U_0(0)\,h/\varepsilon =$ constant $= -\psi_0 b\bar{U}_0$ or

$$y = -\psi_0 - \frac{U_0(0)}{b\bar{U}_0}\,\frac{h_0}{\varepsilon}\,e^{-|x|}. \tag{3.4}$$

The solution φ given in equation (3.3) corresponds to a streamline equation:

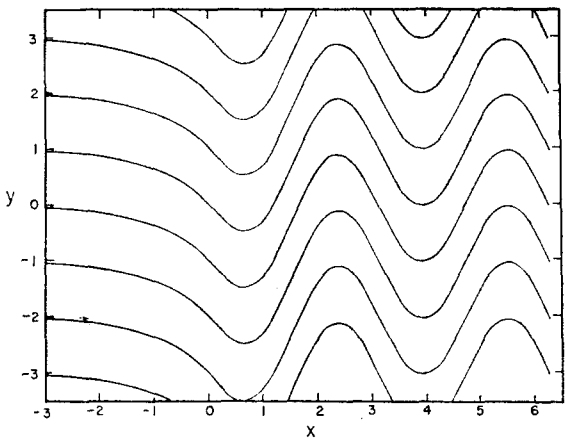

Fig. 1. Contours of ψ for the interaction with a meridionally-oriented ridge. The ridge crest line is along $x = 0$ and the ridge height is proportional to exp $(- | x |)$; $b\bar{U}_0 = 1{\cdot}0$.

$$y = -\psi_0 - \frac{U_0(0)}{1 + b\bar{U}_0}\frac{h_0}{\varepsilon}$$

$$\begin{cases} e^x & x < 0 \\ e^{-x} + 2(b\bar{U}_0)^{-\frac{1}{2}}\sin[(b\bar{U}_0)^{\frac{1}{2}}x] & x > 0. \end{cases} \quad (3.5)$$

The effect of the weak inertia is evident upon comparing equation (3.4) and equation (3.5). For $x < 0$, inertia keeps the streamlines from deflecting as much as the f/H contours [because $b\bar{U}_0/(1 + b\bar{U}_0) < 1$]; while downstream inertial overshoot leaves the streamlines oscillating about the corresponding asymptotic f/H contour.

The streamlines in Fig. 1 bring to mind the dynamic topography contours GORDON and BYE (1972) presented. The circumpolar current crosses a mid-ocean ridge in the South Pacific and then appears to undergo a quasi-steady meandering downstream of it. They indicated the wavelength to be about 1000 km. Assuming the waves to be stationary barotropic Rossby waves, they computed a mean flow velocity (from $\lambda = 2\pi\sqrt{\beta/U}$) of 50 cm s^{-1}. The present model gives a somewhat different wavelength of

$$\lambda = 2\pi\, L(b\bar{U}_0)^{-1/2} \quad (3.6)$$

or using equations (2.1), 2.2), and (2.17)

$$\lambda = \frac{\int_0^H U^2(z')dz'}{\beta\int_0^H U(z')dz'} . \quad (3.7)$$

Given density information and hence the geostrophic velocity field from a meridional section across the meander, equation (3.7) could be used to estimate bottom velocity; i.e. the density field determines $U(z')$ to within an additive constant, and equation (3.7) then becomes an equation for this constant in terms of the density field, β and λ. This calculation was not made for two reasons: the non-synoptic nature of the data used in the GORDON and BYE (1972) paper makes the error bars of estimating λ excessively large, and the stations spacings along the meridional section in this area are rather large, so that the geostrophic velocity field is not well determined.

4. ZONAL RIDGES

The motivation for this particular example is CALLAHAN's (1971) paper on the velocity field south of Australia. There is a zonally oriented mid-ocean ridge to the south and southwest of Australia, and Callahan examined data from five deep, nearly meridional sections across the ridge in the Australian sector. Within the broad eastward drift of the Antarctic Circumpolar Current he consistently found a high baroclinic velocity core embedded on the northern (equatorward) flank of the ridge, and a low baroclinic velocity region, sometimes even westward flow, on the southern flank. He points out that KORT (1963) observed a similar velocity structure in the region south of Africa, where another mid-ocean ridge runs zonally for some distance. He also reported bottom current meter measurements from the 132°E section, *Eltanin* Cruise 41 (ANONYMOUS, 1972), which indicated a reversed (westward) zonal velocity component of almost 6 cm s^{-1} near the ridge crest.

Within the framework of the present model the effect of such a zonally oriented ridge can be examined by using the following idealized topography:

$$h = h_0 \begin{cases} e^{+c^2x}e^{-|y|} & x < 0 \\ e^{-|y|} & x > 0 \end{cases} . \qquad (4.1)$$

Using the constraint of no waves at $x \to -\infty$, the solution to equation (2.18) with this h is:

$$\varphi = -U_0(0)\ \frac{h_0}{\varepsilon}\ e^{-|y|}$$

$$\begin{cases} (k^2 + c^4)^{-1}e^{c^2x} & x < 0 \\ (k^2)^{-1}[1 - c^4(k^2 + c^4)^{-1}\cos kx \\ + c^2k(k^2 + c^4)^{-1}\sin kx] & x > 0, \end{cases} \qquad (4.2)$$

where $k^2 = 1 + b\bar{U}_0$, and it will be assumed that $U_0(0) > 0$.

If $c^2 \ll 1$ (and $c^2k \ll 1$) then φ has the simple form:

$$\varphi = -U_0(0)\ \frac{h_0}{\varepsilon}\ \frac{e^{-|y|}}{k^2} \begin{cases} e^{c^2x} & x < 0 \\ 1 & x > 0 \end{cases} . \qquad (4.3)$$

The zonal velocity field corresponding to equation (4.3) is obtained from equation (2.13) and the second of equations (2.7), which, dropping the superscript (0), gives:

$$u = U_0(z)\,(1 - \varphi_y)$$

$$= U_0(z) - U_0(z)U_0(0)\ \frac{h_0}{\varepsilon}\ \frac{e^{-|y|}}{k^2}$$

$$\begin{cases} e^{c^2x}\mathrm{sgn}(y) & x < 0 \\ \mathrm{sgn}(y) & x > 0 \end{cases} , \qquad (4.4)$$

where $\mathrm{sgn}(y) = +1$ for $y > 1$ and -1 for $y < 1$. Thus as the current rides up the gradually rising exponential skirt upstream of $x = 0$ it is slowly intensified on the equatorward side of the ridge, with a slow flow region on the poleward side. If $U_0(0)\ h_0/\varepsilon k^2 > 1$, then the flow reverses on the poleward side of the ridge. This structure is in agreement with CALLAHAN's (1971) observations.

In the limit $c^2 \gg 1$, the x dependence of h, equation (4.1), is just a step function, and equation (4.2) becomes

$$\varphi = -U_0(0)\ \frac{h_0}{\varepsilon k^2}\ e^{-|y|} \begin{cases} 0 & x < 0 \\ [1 - \cos kx] & x > 0 \end{cases} . \qquad (4.5)$$

The flow still intensifies on the equatorward side, but because of the finite north–south velocities induced, the β-plane again exhibits its spring-like nature, and the streamlines meander downstream of $x = 0$. Isolated stagnation points ($\mathbf{q} = 0$) occur on the poleward side if h_0/ε is greater than:

$$\left(\frac{h_0}{\varepsilon}\right)_c = \frac{k^2}{2U_0(0)}. \qquad (4.6)$$

In Fig. 2 streamlines are shown for $h_0/\varepsilon = (h_0/\varepsilon)_c$ and $2(h_0/\varepsilon)_c$. Immediately downstream of $x = 0$, the streamlines turn anticyclonically, but because of the finite inertia, they overshoot their new equilibrium latitudes and then oscillate in x. The zonal velocity averaged over a wavelength in x is the same as that given in equation (4.4) for $x > 0$.

The second case shown in Fig. 2 corresponds to twice the critical height. Now there is an array of cyclonic eddies on the poleward side of the ridge, with region of westward directed flow within each. GORDON and BYE (1972) commented that the data from the region south of Australia (the same area as Callahan's) do not indicate a continuous westward drift on the poleward side of the ridge, but rather 'a series of filaments of westerly flow'. However, the data do not seem to be dense enough in space or time to determine whether the spatial periodicity indicated in Fig. 2 actually exists along the ridge south of Australia (see Fig. 8).

In Fig. 3 vertical sections of the zonal velocity component are presented for the same two values of h_0/ε as in Fig. 2. In each case the section runs north–south and passes through the stagnation point at $kx = \pi$. The sections can alternatively be interpreted as representing the velocity field of the $c^2 \ll 1$ solution, equation (4.4), for $x > 0$ and

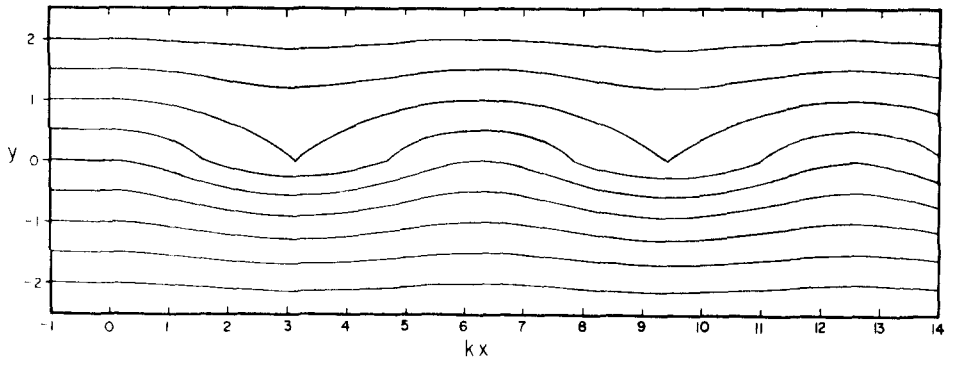

Fig. 2a.

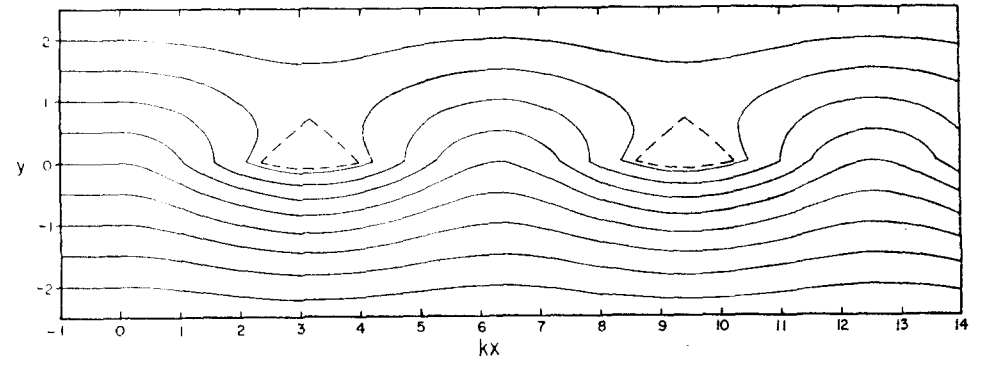

Fig. 2b.

Fig. 2. Contours of ψ for the interaction with a zonally-oriented ridge. The ridge crest line is along $y = 0$; there is topography only downstream of $x = 0$, where it is independent of x; the ridge height is proportional to exp $(-|y|)$. (a) corresponds to a ridge height equal to that of equation (4.6) while (b) is twice that value. The dashed lines are the $\psi = -1{\cdot}693$ contours, the outermost closed ψ contours, which exhibit a stagnation point at $kx = (2n - 1)\pi$, $y = 0{\cdot}693$. This streamline originates at $y = +1{\cdot}693$ upstream; this segment is not shown. Positive y is poleward.

$(h_0/\varepsilon) = k^2/U_0(0)$ and $2k^2/U_0(0)$. The particular $U_0(z)$ used in the calculation was

$$U_0(z) = 1{\cdot}571 \exp [-1{\cdot}099(1 - z)], \quad (4.7)$$

which has the property $U_0(1)/U_0(0) = 3{\cdot}0$ and has maximum vertical shear and curvature at the surface. This velocity ratio is roughly what Callahan observed (combined bottom current meter data and geostrophic velocity calculations from density data), while the strongest vertical shear and curvature were near the surface. The zonal velocities calculated from equation (4.2) are discontinuous at $y = 0$, reflecting the discontinuity in $\partial h/\partial y$ there. A smoothly varying topography would have a smoothly varying velocity field, still intensified on the equatorward side of ridge crests as in the present example.

The mechanism of the current alteration in the present example should be contrasted with THOMPSON's (1971a, b) mechanism. In the present example the current intensification on the equatorward side of the ridge and slowing on the poleward side of the ridge represent basically the tendency to follow lines of constant f/H. Stationary Rossby waves can occur, but, as the $c^2 \ll 1$ example showed, they are not responsible for the mean current pattern along the ridge. THOMPSON (1971a, b) pointed out that given an existing slowly meandering eastward current over a north–south linearly sloping bottom, barotropic Rossby waves propagating away from the meander region will converge momentum into the meander region if the ocean depth shoals in the poleward direction, but they will remove momen-

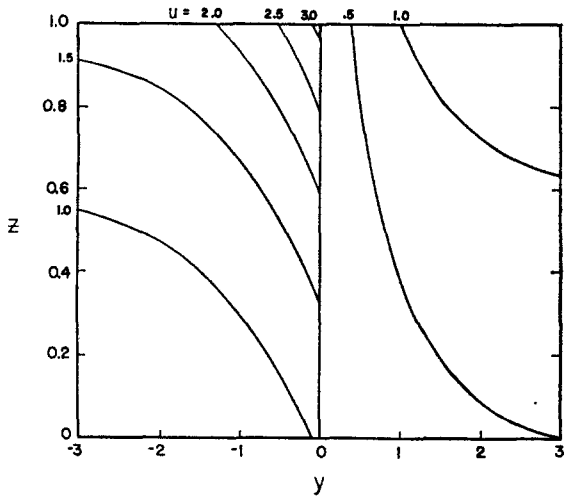

Fig. 3a.

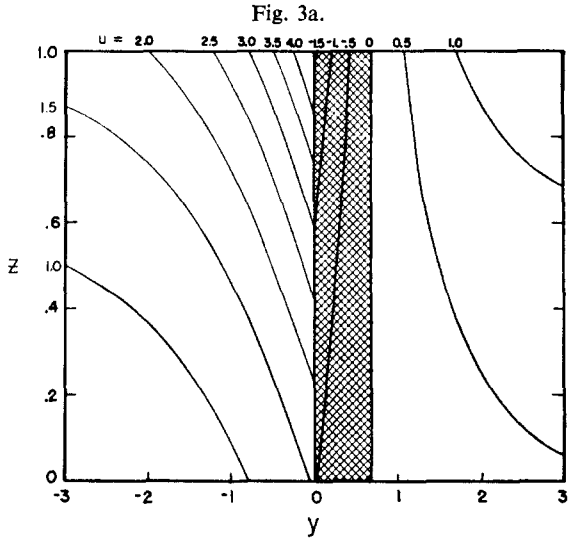

Fig. 3b.

Fig. 3. Zonal velocity sections through $kx = \pi$, for the same case as illustrated in Fig. 2. Positive y is poleward. The vertical dependence of the velocity field is exponential in character, given by equation (4.7). The contours are constant speed lines. The zonal velocity is discontinuous at $y = 0$. (a) corresponds to $(h_0/\varepsilon)_c$, equation (4.6) and Fig. 2(a); (b) corresponds to $2(h_0/\varepsilon)_c$ and Fig. 2(b). The cross-hatched region is westward flow.

tum from the region if the ocean depth deepens poleward rapidly enough to counteract the planetary β effect. This mechanism is not active in the present model; it could play a role in adjustment problems: response of the current system to changes in the approaching flow velocity, or problems with either time-dependent forcing or some active instability mechanism generating time-dependent meanders and eddies.

Restricting attention to the $c^2 \gg 1$ solution, equation (4.5), what happens if the topography amplitude changes abruptly at $x = x_0$, i.e.

$$h_0 = \begin{matrix} h_0 & 0 < x < x_0 \\ h_0\gamma & x_0 < x \end{matrix} \quad ? \tag{4.8}$$

The solution for $x < x_0$ remains unchanged, i.e. φ in equation (4.5); downstream φ becomes:

$$\varphi = -\frac{U_0(0)}{k^2}\frac{h_0}{\varepsilon} e^{-|y|}[\gamma - m\sin(kx - \zeta)], \tag{4.9}$$

where

$$m = \sqrt{[1 + (1-\gamma)^2 - 2(1-\gamma)\cos kx_0} \tag{4.10}$$

and

$$\zeta = c + m^{-1}\left\{\frac{(1-\gamma)\sin kx_0}{1-(1-\gamma)\cos kx_0}\right\}. \tag{4.11}$$

If, in particular, equation (4.9) is examined for the case $\gamma = 0$, i.e. no topography downstream of x_0, isolated stagnation points occur in the wake at values of x satisfying: $kx - \zeta = n\pi/2$ ($n = 1, 2, 3, \ldots$, restricted to $x > x_0$), if

$$\frac{h_0}{\varepsilon} > \frac{k^2}{m} = \frac{k^2}{\sqrt{2}}\frac{1}{\sqrt{(1-\cos kx_0)}}. \tag{4.12}$$

This value lies in the range $(k^2/2, \infty)$. Because the flow for $x < x_0$ has stagnation points if $h_0/\varepsilon > k^2/2$, three distinct configurations occur: no stagnation points anywhere, stagnation points only for $0 < x < x_0$, and stagnation points for all $x > 0$. In Fig. 4 streamlines are shown for the case shown in Fig. 2(b): $h_0/\varepsilon = k^2$, but with the ridge truncated at $x_0 = 3\pi/(2k)$ (note that if $x_0 = 2\pi/k$, there is no disturbance downstream).

There is now a stationary vortex street array downstream of the ridge: cyclonic eddies on the poleward side, anticyclonic eddies on the equator side of $y = 0$. This wake is of a non-diverging variety—the structure is simply periodic in x. This is not a general feature for flow past isolated

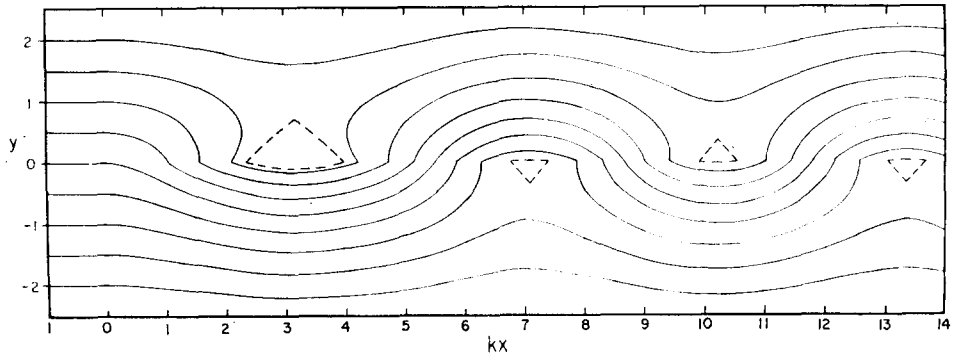

Fig. 4. Contours of ψ for the interaction with a finite length zonally oriented ridge. Conditions identical to Fig. 2(b), except the ridge ends at $kx = 3\pi/2$. The smaller dashed ψ contours correspond to $\psi = \pm 1{\cdot}347$, and they originate at $y = \mp 1{\cdot}347$. They are streamlines with stagnation points for the wake, and thus are the outermost closed ψ contours.

topographic features. Indeed, in the next section the flow past an isolated circular bump is examined—the traditional Taylor column geometry. A meandering wake is still found, but it is of a radial character and thus decays away from the bump. Instead of an infinite number of eddies in a street configuration only a finite number of eddies are found.

5. ISOLATED BUMP

The particular topography used in this section will be an axisymmetric bump with a step-function radial dependence:

$$h = h_0 \begin{cases} 1 & r < 1 \\ 0 & r > 1 \end{cases} \tag{5.1}$$

(cylindrical coordinates being used throughout this section with θ measured counterclockwise from x direction).

The solution to equation (2.18) with this h, constrained to have no waves far upstream, i.e.

$$r^{\frac{1}{2}}\varphi \to 0 \quad \text{at} \quad r \to \infty,$$

$$\pi/2 < \theta < 3\pi/2, \tag{5.2}$$

and also to have continuous φ and $\nabla\varphi$ at $r = 1$, is identical to that given by McCartney (1975) for the case of a homogeneous fluid on a β-plane. In the present notation this solution is:

$$\varphi = -\frac{U_0(0)}{m}\frac{h_0}{\varepsilon}\left\{\Sigma + \begin{cases} m^{-1} + \frac{\pi}{2}Y_1(m)J_0(mr) & r < 1 \\ +\frac{\pi}{2}J_1(m)Y_0(mr) & r > 1 \end{cases}\right., \tag{5.3}$$

where $m = (b\bar{U}_0)^{\frac{1}{2}}$, J_0, and J_1 are Bessel functions of the first kind, Y_0 and Y_1 are Bessel functions of the second kind, and

$$\Sigma \equiv 2J_1(m)\sum_{n=1}^{\infty}\frac{J_{2n-1}(mr)\cos[2n-1)\varphi]}{2n-1}. \tag{5.4}$$

The Σ term asymptotically cancels the $Y_0(mr)$ term on the upstream half plane, thus satisfying the no upstream wave condition [equation (5.2)].

A general expression for the critical height for which this solution has a stagnation point cannot be obtained from this solution. In Fig. 5 streamlines are shown for the case of $m = 1$ and values of $U_0(0)h_0/\varepsilon = 2{\cdot}0,\ 4{\cdot}0,\ 6{\cdot}0$. In all three cases there is a slow flow region over the upstream equatorward quadrant of the bump. For the shortest bump, there are no closed streamlines in this region, but for the two taller bumps there are. These closed streamlines are just the β-plane counterpart of Ingersoll's (1969) f-plane inertial Taylor columns; indeed, his solution* can be ob-

*Only his inviscid solution is obtained; the solution he presented with a stagnant Taylor column—using the bottom frictional argument discussed in Section 2—is not obtainable from equation (5.3).

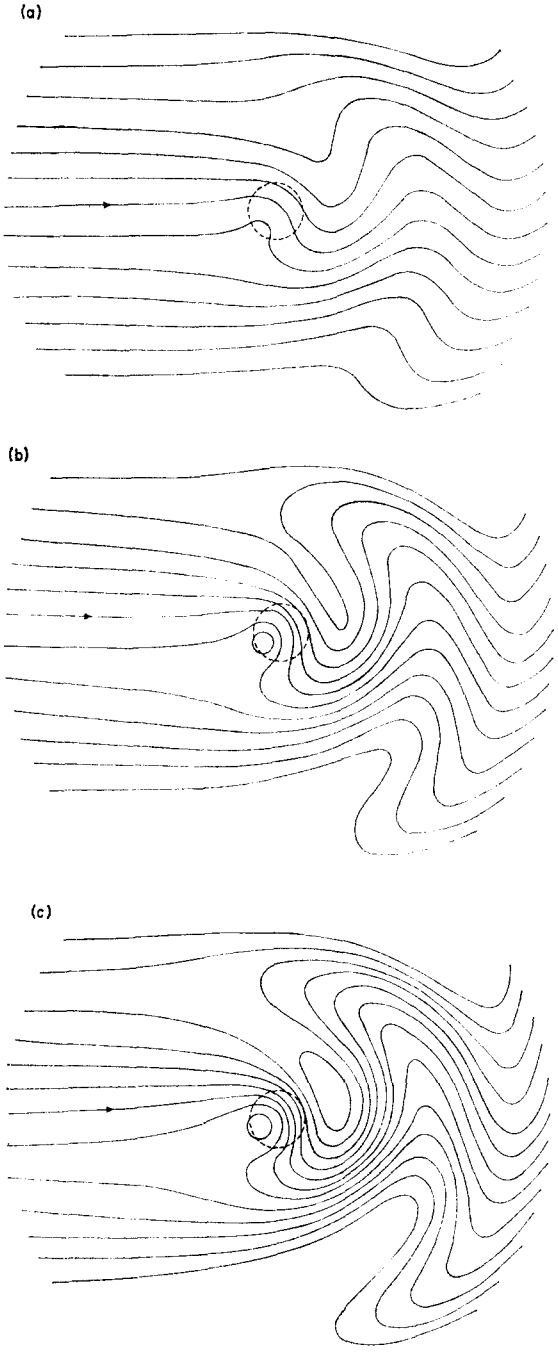

Fig. 5. Contours of ψ for the interaction with an isolated circular flat-topped bump. The bump is indicated by the dashed contour. $b\bar{U}_0 = 1$, and $U_0(0)h_0/\varepsilon =$ (a)2, (b)4, and (c)6. The closed contour in (b) is the $\psi = 2$ contour, while the smaller one in (c) is $\psi = 2$, the larger $\psi = -5$. The outermost closed contours in each case were not computed due to the complexity of equation (5.3).

tained from the present one by taking the double limit $b \to 0$, $S \to 0$. HOGG's (1973) weakly stratified Taylor column solution is recovered from the present solution by taking only the limit $b \to 0$. Returning to Fig. 5, on the downstream poleward side of the bump there is another slow flow region —a cyclonic meander. As the bump height increases, the amplitude of this meander increases until it pinches off forming a cyclonic eddy. Similarly, there is an anticyclonic meander to the downstream equatorward side that pinches off to form an anticyclonic eddy. The meander in Fig. 5b resembles GORDON's (1972, 1975) pictures of the interaction of the Antarctic Circumpolar Current with the Macquarie ridge complex southwest of New Zealand. From the depth of the salinity maximum core layer, he has inferred that the dynamic topography exhibits an anticyclonic loop over the southernmost end of the ridge system (near 158°W longitude and 58°S latitude). In the more recent paper he contours an anticyclonic eddy over the ridge tip. In both papers a cyclonic meander is contoured downstream of the ridge tip.

Another feature of the solution φ in equation (5.5) deserves comment. If the value of m is such that $J_1(m) = 0$, then for $r > 1$, $\varphi \equiv 0$. This gives a stationary trapped wave disturbance over the bump and no disturbance outside the bump. Two examples of this resonance phenomenon were shown in MCCARTNEY (1975).

6. PERTURBED DENSITY FIELDS

The three-dimensional density field corresponding to the φ solutions presented in the previous sections is immediately obtainable from equations (2.4) and (2.13), which give:

$$\frac{\rho' - \rho'_0}{\Delta\rho} = \rho_s(z) + \frac{\varepsilon}{S}\frac{dU_0(z)}{dz}[y - \varphi]. \qquad (6.1)$$

If the restriction to $dU_0(z)/dz > 0$, i.e. maximum speeds at surface, is made, then the plots of $\psi(x, y)$ presented in Figs. 1, 2, 4, and 5 also represent the intersection of isopyncal surfaces with a horizontal surface, with the density values on the contours increasing with increasing y,

except in those regions with reversed flow. Cyclonic eddies have a local density maximum (cold core) while anticyclonic eddies have a local density minimum (warm core). The origin of these extremes in density can be understood by envisioning a startup process in which the topography is 'created' at time zero. The streamlines, initially straight, feel the topography, and deflect with time until a streamline meanders sufficiently strongly to close back upon itself. If the meander is cyclonic it traps a core of more dense water originating from further poleward, much as a Gulf Stream meander pinches off forming a ring with slope water in the core (FUGLISTER, 1972). Similarly, an anticyclonic eddy pinches off a core of warm water originating from further equatorward.

Returning to Fig. 2, it is seen that the interaction of the current with the semi-infinite cusp-cross-section ridge has produced a string of cyclonic cold core eddies, while the finite length ridge in Fig. 4 has an eddy street of alternate cyclonic cold core and anticyclonic warm core eddies. The isolated bump in Fig. 5c has an anticyclonic, warm core eddy (Taylor column) over the bump, and a cyclonic cold core eddy to the downstream poleward side.

For fixed $x = x_0$, $z = z_0$, and with φ given by equation (4.5), for the zonal exponential cusp-cross-section ridge, equation (6.1) has the form

$$\frac{\rho'(x_0, y, z_0) - \rho_0'}{\Delta\rho} = A + By + C\,e^{-|y|}, \qquad (6.2)$$

with A, B, and C being positive constants depending on x_0 and z_0. The values of the constants are such that the y variation in equation (6.2) is monotonic only if $(h_0/\varepsilon) < (h_0/\varepsilon)_c$ given by equation (4.6). For larger h_0/ε, there can be local extremes in density as discussed above. In Fig. 6 plots of the density relation in equation (6.2) are presented for two values of the ratio C/B, 1·0 and 2·0, corresponding to north–south sections through the stagnation points, at some depth z, of Figs. 2a and 2b. In Fig. 7 data from two *Eltanin* sections, 140 and 128°E (Stas. 891 to 910 and 869 to 877 in JACOBS, BRUCHHAUSEN and BAUER, 1970) are presented for comparison with Fig. 6, in the form of plots of σ_t at various fixed depths versus latitude. The reversal in slope on the northern end of the 128°E section is associated with an anticyclonic gyre in the Great Bight. At Sta. 874 the upper 600 m were essentially homogeneous at a temperature of 8·23 to 8·33°C and σ_t of 26·93 to 26·94.

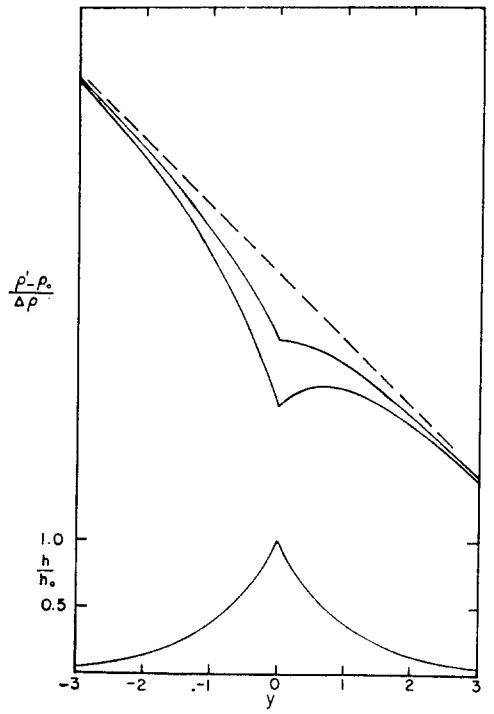

Fig. 6. Plot of the variation of density with latitude at fixed depth for $kx = \pi$ in Fig. 2. The dashed line is the density variation corresponding to the uniform approaching flow. The upper curve corresponds to Fig. 2(a), the lower to Fig. 2(b). The ridge profile is shown at the bottom.

To investigate further the relation between the high velocity core and the ridge system south and southwest of Australia that Callahan first noted, the *Eltanin* data collection for the area, as contained in reports by JACOBS, BRUCHHAUSEN and BAUER (1970), JACOBS, BRUCHHAUSEN, ROSSELDT, GORDON, AMOS and BELLIARD (1972), and JACOBS, BAUER, BRUCHHAUSEN, GORDON, ROOT and ROSSELOT (1974), were examined. The values of σ_t at 1000 m were specifically examined. In Fig. 8 the locations of station pairs with σ_t differences at 1000 m greater than or equal to that

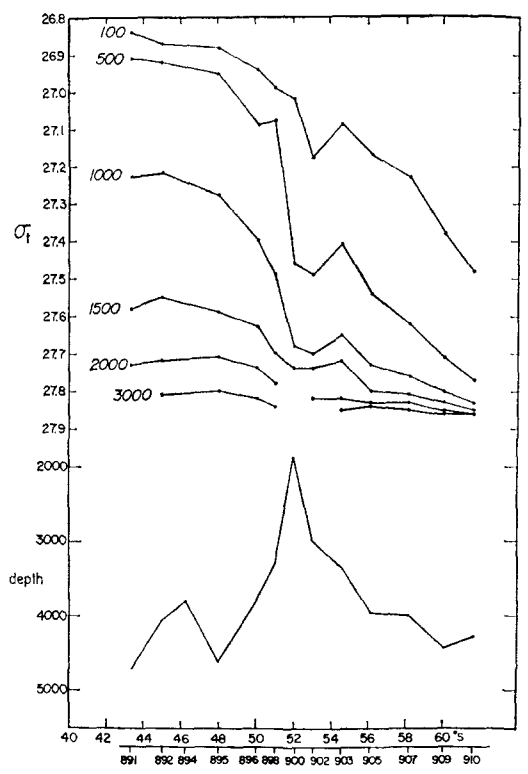

Fig. 7a.

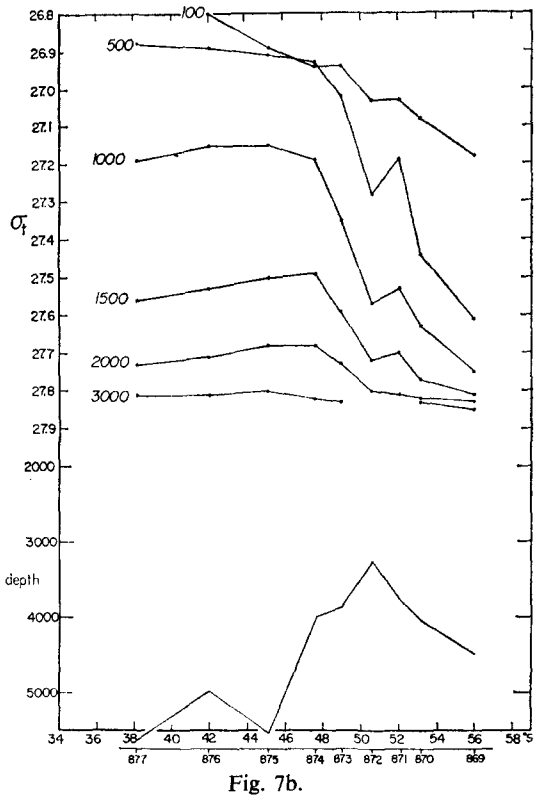

Fig. 7b.

Fig. 7. Plots of density, σ_t, versus latitude at various values of depth, for sections across the zonal ridge south of Australia. Poleward (south) is to the right. The bottom contour is an idealization of the ridge cross-section; simply straight line segments connecting the station depth soundings. (a) is a section along 140°E, *Eltanin* Stas. 891 to 910, (b) is a section along 128°E, *Eltanin* Stas. 877 to 869. Note the dip in the lines immediately over the ridge crest (Stas. 800 and 872), throughout the water column, the strong gradients to the equatorward (north) side, and reversed gradients to the poleward (south) side, and compare to Fig. 6.

corresponding to 0·1 per degree latitude are plotted on a bottom topographic chart derived from that of HEEZEN, THARP and BENTLEY (1972). On a given section generally only one or two station pairs satisfy the criterion. Also shown on the chart are those stations pairs showing a σ_t gradient reversal associated with a westward baroclinic velocity. After some adjustment at the western end, the flow settles down into the pattern of a high velocity core on the northern flank of the ridge and intermittent reversed flow on the southern flank. Only the ridge crest center line is indicated; this is the center of the irregular, less than 3000-m band that defines the ridge in the Heezen, Tharp, and Bentley chart. This band is typically 2 or 3 degrees wide. East of 140°E, things are complicated by the Tasman Plateau, which rises to less than 1000 m around 153°E and 47°S, the Macquarie ridge system along 160°E between 51° and 59°S (viz. GORDON, 1972), and the massive Campbell Plateau (viz. GORDON, 1975). All three appear to have local high velocity regions and local flow reversals. The ridge axis has dipped well to the south in this sector (over 12° in latitude). The 0·1 per degree criterion is probably not appropriate this far south because of the increased homogeneity of the water column: GORDON (1975) indicates a high velocity core on the northern flank of the ridge between 62 and 63°S along 170°E, which the present criterion misses because of the relatively homogeneous water at 1000 m this far south.

The vertical density gradient can be obtained by differentiating equation (6.1) with respect to z:

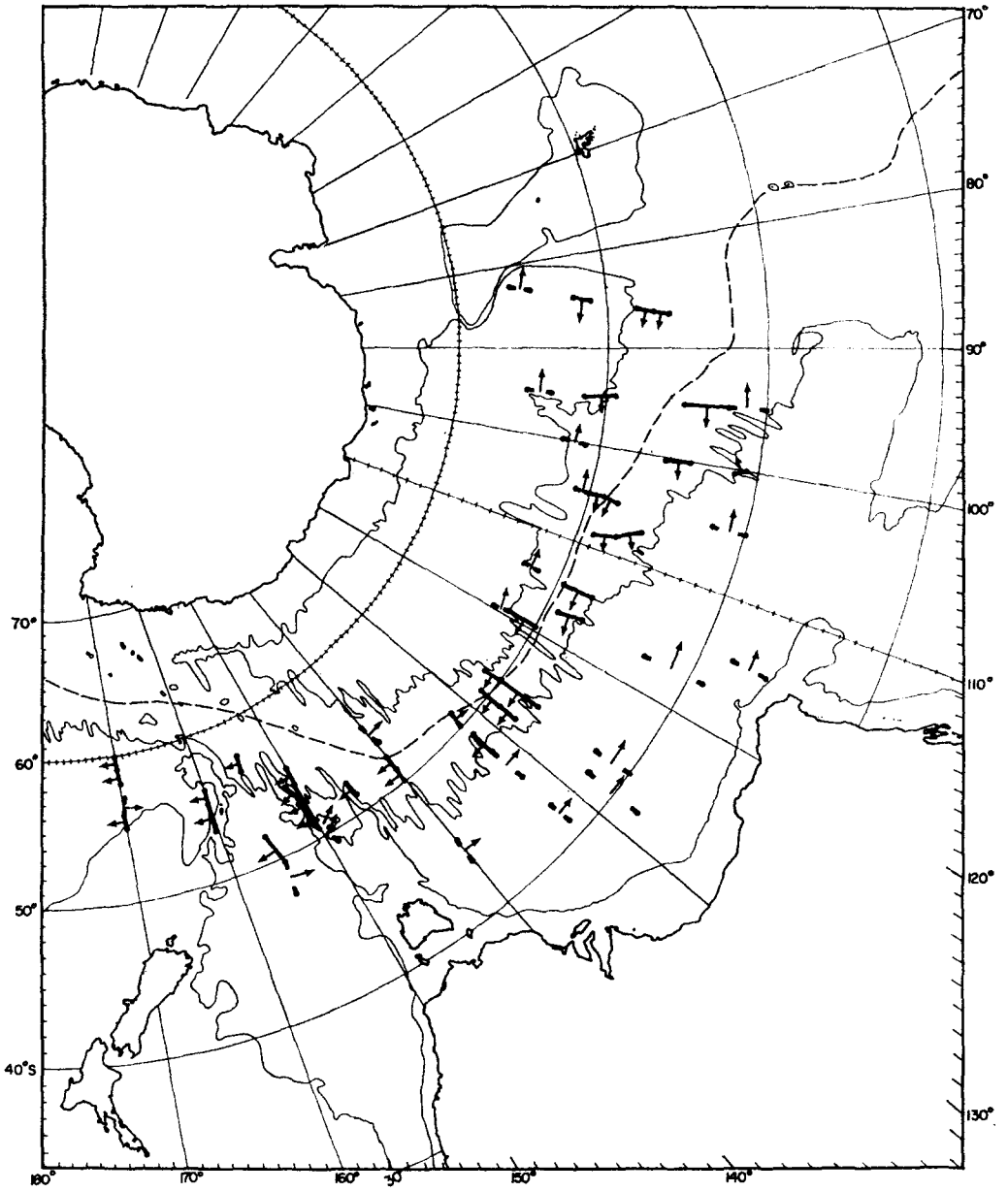

Fig. 8. Locations of the U.S.N.S. *Eltanin* station pairs corresponding to steep gradients of σ_t at 1000 m ($> 0{\cdot}1$ per degree latitude) on north–south sections in the region between 170 and 80°E. These are indicated by eastward directed arrows between station dots. The light lines are the 4000-m contours from HEEZEN, THARP and BENTLEY (1972); while the dashed line is the centerline of the ridge crest, the band < 3000 m on their chart. The station pairs with westward directed arrows are those with reversed σ_t gradients at 1000 m, and occur in two main areas: intermittently along the southern side of the ridge and in the Great Bight region south of Australia. The data plotted in Fig. 7 from 140 and 128°E can be compared with this chart for additional orientation.

$$\frac{1}{\Delta\rho}\frac{\partial\rho'}{\partial z} = \frac{d\rho_s(z)}{dz} + \frac{\varepsilon}{S}\frac{d^2U(z)}{dz^2}\,[y-\varphi]. \quad (6.3)$$

This gradient has a local extreme (if $d^2U(z)/dz^2 \neq 0$) at the same horizontal location as any stagnation points in the flow field. Because the right-hand side of equation (6.3) can be written in the form $f(z) - g(z)\psi$, the plots of $\psi(x, y)$ in Figs. 1, 2, 4, and 5 also represent contours, in a horizontal plane, of constant vertical density gradient. The sense of the extreme at the stagnation point is determined by the sign of ψ at the stagnation point (ψ_{st}) and by the sign of $d^2U_0(z)/dz^2$. For $d^2U_0(z)/dz^2 < 0$ (which might be expected in the near-surface region above the main pycnocline), the vertical gradient will have a local maximum (minimum) when $\psi_{st} > 0$ (< 0). The local maximum corresponds to a local minimum in vertical stability. Thus in the figures, the anticyclonic eddies, which have corresponding $\psi_{st} > 0$, will have [if $d^2U_0(z)/dz^2 < 0$] a relatively low vertical stability. It might be supposed that this, coupled with the fact that the eddies represent warmer water entrained from lower latitudes, would make these anticyclonic eddies particularly susceptible to surface cooling and overturning. For regions of the water column where $d^2U_0(z)/dz^2 > 0$ (typically below the main pycnocline), the lowest local vertical stability is associated with the cyclonic eddies (with corresponding $\psi_{st} < 0$).

7. CONCLUSIONS

The solutions presented in the previous section show several features that have been observed in the Southern Ocean. Upon approaching a meridional ridge, a broad eastward current is shown to deflect initially equatorward, then downstream of the ridge crest to meander (Fig. 1); much as GORDON and BYE (1972) indicated occurs in the south central Pacific Ocean. A zonally oriented ridge causes the current to be intensified on the equatorward side of the ridge crest, and slowed or reversed on the poleward side (Figs. 2, 3, 4, and 6). This agrees with CALLAHAN's (1971) observations on the southeast Indian Ocean. Finally an isolated bump is shown to force a closed anticyclonic Taylor column over the bump, and an extensive meandering wake downstream (Fig. 5), with a cyclonic meander or eddy to the poleward-downstream dominating the meander pattern. This pattern is similar to what GORDON (1972, 1975) observed over the top of and downstream of the Macquarie ridge.

The model should, however, only be regarded as a first step in an attempt to understand the role of topographic interactions in Southern Ocean dynamics. To solve the problem analytically it was necessary to restrict the class of basic currents to those horizontally uniform. If the more general approaching flow $p^{(0)} \to -U_0(z)g(y)$ is used, then $p^{(0)}$ still has the separable form given in equation (2.10); however, the steps leading from equation (2.13) to equation (2.15) will now, in general, yield a nonlinear equation for ψ, and recourse to numerical methods will probably have to be had.

Another area for further investigation is the extension to $h_0 = O(1)$ rather than just $O|\varepsilon|$ as in the present work. Do the present solutions with disturbance linearily proportional to h_0/ε continue to grow for $h_0 = O(1)$ or does the disturbance reach some limiting value for some intermediate value of h_0? Is this limiting process inherent in a purely inviscid $h_0 = O(1)$ model, or must some mechanism such as INGERSOLL's (1969) bottom frictional spindown for large time be included?

As a related problem it also would be of interest to investigate the equivalent inviscid initial value problem to see first whether the large time solution approaches the present steady-state solutions, and secondly to observe the startup process and the details of the eddy pinch-off process. Are the large amplitude meander and eddy patterns always stationary, or do temporally periodic fields or instabilities occur?

The model as it stands can be used also to examine the flow through a channel with parallel walls and various kinds of bottom topography. The analysis is more complex because of the requirement that $\varphi = 0$ at the channel walls, but is straightforward. This kind of model has some relevance for the flow through the Drake Passage.

Acknowledgements—I would like to express my thanks to the Woods Hole Oceanographic Institution for its support of this work through a post-doctoral scholarship. Additional support was provided by the Oceanography Section of the National Science Foundation, Grant No. GA-35447, and the Office of Naval Research, Contract No. N00014-74-C-0262 NR083-004.

REFERENCES

ANONYMOUS (1972) Physical and chemical data from Cruise 41 of U.S.N.S. *Eltanin* in the Southern Ocean between Australia and Antarctica 20 December 1969–16 February 1970. Scripps Institution of Oceanography Reference 72-19, 57 pp.

CALLAHAN J. E. (1971) Velocity structure and flux of the Antarctic Circumpolar Current south of Australia. *Journal of Geophysical Research*, **76**(24), 5859–5870.

CLARK R. A. and N. P. FOFONOFF (1969) Oceanic flow over varying bottom topography. *Journal of Marine Research*, **27**(2), 226–240.

EKMAN V. W. (1923) Über Horizontalzirkulation bei winderzeugten Meeresströmungen. *Arkiv för matematik, astronomi och fysik*, **17**(26), 1–74.

FUGLISTER F. C. (1972) Cyclonic rings formed by the Gulf Stream 1965–66. In: *Studies in physical oceanography*, A. L. GORDON, editor, Gordon & Breach, Vol. 1, pp. 137–168.

GORDON A. L. (1972) On the interaction of the Antarctic Circumpolar Current and the Macquarie Ridge. In: *Antarctic oceanology* II: *the Australian–New Zealand sector*, Antarctic Research Series, **19**, D. E. HAYES, editor, American Geophysical Union, 71–78.

GORDON A. L. (1975) An oceanographic section along 170°E. *Deep-Sea Research*, **22**, 357–377.

GORDON A. L. and J. A. T. BYE (1972) Surface dynamic topography of Antarctic waters. *Journal of Geophysical Research*, **77**(30), 5993–5999.

HEEZEN D. E., M. THARP and C. BENTLEY (1972) Morphology of the Earth in the Antarctic and Sub-Antarctic. *Antarctic Map Folio Series*, **16**, American Geographical Society.

HOGG N. G. (1973) On the stratified Taylor column. *Journal of Fluid Mechanics*, **58**(3), 517–537.

INGERSOLL A. P. (1969) Inertial Taylor columns and Jupiter's Great Red Spot. *Journal of Atmospheric Sciences*, **26**(4), 744–752.

JACOBS S. S., P. M. BRUCHHAUSEN and E. B. BAUER (1970) *Eltanin* Reports. Cruises 32–36, 1968. Lamont-Doherty Geological Observatory of Columbia University. Technical Report 1-CU-1-70.

JACOBS S. S., P. M. BRUCHHAUSEN, F. L. ROSSELOT, A. L. GORDON, A. F. AMOS and M. BELLIARD (1972) *Eltanin* Reports, Cruises 37–39, 1969; 42–46, 1970. Lamont-Doherty Geological Observatory of Columbia University Technical Report 1-CU-1-72.

JACOBS S. S., E. B. BAUER, P. M. BRUCHHAUSEN, A. L. GORDON, T. F. ROOT and F. L. ROSSELOT (1974) *Eltanin* Report. Cruises 47–50, 1971; 52–55, 1972. Lamont-Doherty Geological Observatory of Columbia University Technical Report CU-2-74.

KORT V. G. (1963) The water transport of the Southern Ocean. *Okean. Issled*, **10**(8), 5–16.

LIGHTHILL J. J. (1966) Dynamics of rotating fluids: a survey. *Journal of Fluid Mechanics*, **26**(2), 411–413.

MCCARTNEY M. S. (1975) Inertial Taylor columns on a beta-plane. *Journal of Fluid Mechanics*, **68**(1), 71–95.

MCINTYRE M. E. (1968) On stationary topography-induced Rossby-wave patterns in a barotropic zonal current. *Deutsche hydrographische Zeitschrift*, **21**(5), 203–214.

NEUMANN G. (1960) On the effect of bottom topography on ocean currents. *Deutsche hydrographische Zeitschrift*, **13**(3), 132–141.

PORTER G. H. and M. RATTRAY (1964) The influence of variable depth on steady zonal barotropic flow. *Deutsche hydrographische Zeitschrift*, **17**(4), 164–174.

SVERDRUP H. U. (1941) The influence of bottom topography on ocean currents. In: *Applied Mechanics, Th. v. Kármán Anniversary Volume*, pp. 66–75.

THOMPSON R. O. R. Y. (1971a) Why there is an intense eastward current in the North Atlantic but not in the South Atlantic. *Journal of Physical Oceanography*, **1**(3), 235–237.

THOMPSON R. O. R. Y. (1971b) Structure of the Antarctic Circumpolar Current. *Journal of Geophysical Research*, **76**(36), 8694.